Chapter 2 Thermal evaluation of multi-glazed windows under *Aw* Köppen climate classification: An analysis by mean of global energy balances

Capítulo 2 Evaluación térmica de ventanas de vidrios múltiples bajo el clima *Aw* de la clasificación de Köppen: Un análisis por balances globales de energía

LÓPEZ-SALAZAR, Samanta[1], LIMA-TÉLLEZ, Thania Guadalupe[2], CHÁVEZ-CHENA, Yvonne[1] and SIMÁ- MOO, Efraín[1]

[1]Tecnológico Nacional de México / CENIDET, Prol. Av. Palmira S/N, Col. Palmira, Cuernavaca, Morelos CP 62490, México
[2]Universidad de Sonora, DIQyM-UNISON, Blvd. Luis Encinas y Rosales S/N, Hermosillo, Sonora, CP 83000, México

ID 1st Author: *Samanta, López-Salazar* / **ORC ID**: 0009-0004-9880-5145, **CVU CONAHCYT ID**: 918135

ID 1st Co-author: *Thania Guadalupe, Lima-Téllez* / **ORC ID**: 0009-0001-1072-8324, **CVU CONAHCYT ID**: 857109

ID 2nd Co-author: *Yvonne, Chávez-Chena* / **ORC ID**: 0000-0003-3348-397X, **CVU CONAHCYT ID**: 37563

ID 3rd Co-author: *Efraín, Simá-Moo* / **ORC ID**: 0000-0001-7601-1273**, CVU CONAHCYT ID**: 83891

DOI: 10.35429/H.2023.8.14.34

S. López, T. Lima, Y. Chávez and E. Simá

* d18ce057@cenidet.tecnm.mx

A. Marroquín, L. Castillo, J. Olivare sand G.Morado (Coord) Engineering Sciences and Applications. Handbooks-©ECORFAN-México, Querétaro, 2023.

Abstract

Nowadays, researchers have proposed the use of multi-glazed window as a strategy to improve the thermal comfort in buildings. Therefore, in this study the effect on the thermal performance of three glazed configurations: single (SW), double (DW), and triple (TW) windows under *Aw* Köppen climate classification was evaluated. The thermal analysis was carried out starting with the modeling of the window conjugate heat transfer by mean the global energy balance method. In this work, the window thermal performance for the warmest and coldest days of the year are presented first, in order to show the temperature and heat flux trends. Based on these results it was observed that the TW decreased the window energy gains by 36.7 % and losses by 8 %. Subsequently, an annual thermal evaluation of the TW is presented in order to show the advantages and disadvantages of positioning the window in different orientations and its potential on energy saving. The highest energy savings were obtained for the north orientation (2.2 $kW \cdot h \cdot m^{-2}$), followed by west (3.6 $kWhm^{-2}$), south (3.9 $kWhm^{-2}$) and east (4.0 $kWhm^{-2}$). On the north orientation, the solar radiation values are low (<400 W/m^2), so the window energy gains are 50% lower than the other orientations, therefore multi-glazed windows are unnecessary.

Thermal evaluation, Numerical study, Heat transfer, Multi-glazed, Thermal comfort

Resumen

Actualmente, los investigadores proponen utilizar vidrios múltiples como una estrategia para mejorar el confort térmico. En este estudio se evaluó el efecto de tres configuraciones de acristalamiento: simple (SW), doble (DW) y triple (TW) en el desempeño térmico de una ventana bajo el clima *Aw* de la clasificación Köppen. El análisis se llevó a cabo a partir del modelado de la transferencia de calor por el método de balances globales de energía. Primero se muestran las tendencias de la temperatura y flujo de calor en el día más cálido y frío del año. Con base en los resultados, la TW redujo la pérdida y ganancia de energía 36.7 % y 8 %, respectivamente. Después, se presentó la evaluación térmica anual de la TW para mostrar el potencial de ahorro de energía en diferentes orientaciones. El mayor ahorro de energía se obtuvo en la orientación norte (2.2 $kW \cdot h \cdot m^{-2}$), seguida del oeste (3.6 $kWhm^{-2}$), sur (3.9 $kWhm^{-2}$), y este (4.0 $kWhm^{-2}$). En la orientación norte, los niveles de radiación son bajos (<400 W/m^2), debido a esto la ganancia de energía de la ventana es 50 % menor que en las otras orientación, por lo tanto, el uso de vidrios múltiples es innecesario.

Evaluación térmica, estudio numérico, transferencia de calor, vidrios múltiples, confort térmico

1. Introduction

Currently, researchers are looking for strategies to save energy, especially in buildings, where people perform their activities 90 % of the day. Energy saving means reducing the building energy needs through the use of efficient systems with a positive cost-benefit balance, in other words, energy saving should not affect people comfort during the development of their activities. Building comfort is established based on three main parameters: noise, lighting quality, and temperature, Figure 1. In order to improve the building comfort, efficient lighting systems, acoustically and thermally insulated systems are required. In addition, improvements in thermal insulation are expected to reduce CO_2 emissions and electricity consumption in the building sector.

Figure 1 Factors that determine the comfort level in buildings

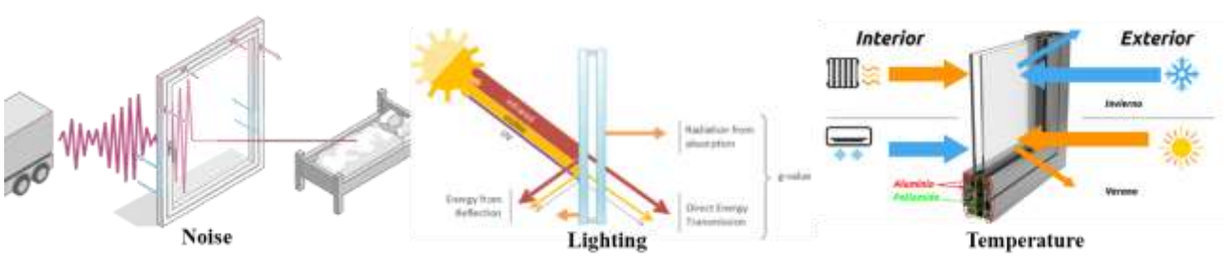

Source: Own Elaboration

In Mexico, the demand for housing is increasing, as well as the ambient temperature due to climate change, therefore, it is necessary to develop thermal insulation strategies and devices that alone improve thermal comfort and avoid the use of ventilation devices, which increase the electricity consumption and environmental pollution, especially in the north and the coasts of the country, where ventilation and air conditioning systems are recurrent (see Figure 2).

In order to reduce the time of use of ventilation devices and improve the building thermal insulation several investigations have been carried out focused on the study of the building envelope elements such as the roof, walls, and windows, and the relationship with the design variables (location, position, and orientation) in order to develop strategies to save energy. According to Bienvenido-Huertas et al.[1], it is necessary to optimize the thermal performance of glaze facades in order to control solar gains and reduce energy demand in buildings.

For the building's envelope, windows are only aesthetic elements, whose function is to allow us to look outside and receive natural light, which improves the people physical and mental health [Vitro[2]]. However, from the thermal approach, the low thermal insulation and the high transmittance value of single glazed increase the window heat transfer rate, and consequently the indoor building temperature. Therefore, conventional windows must be redesigned taking into account the location, climate, and façade orientation in order to improve the windows thermal efficiency and the building thermal comfort. Around the world, researchers have proposed the use of multi-glazed window as a strategy to improve the thermal comfort in buildings.

Figure 2 Climate map by regions, use of air conditioning

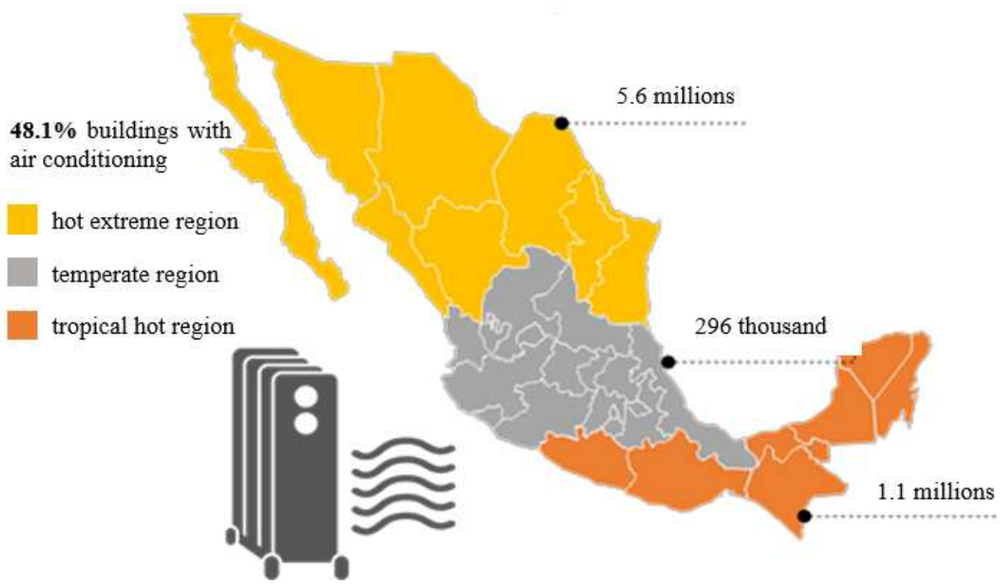

Source: INEGI, 2018

Several investigations have focused on analyzing multi-glazed design parameters such as glazing panes number [Arıcı et al., 2015[3]], encapsulated fluids like air [Gonzalez-Julian et al., 2018[4]] and noble gases [Heydari et al., 2020[5]], phase change materials [Yang et al., 2023[6]], and supplied water [Yamaç and Koca, 2023[7]]. On the other hand, authors such as Huang et al., 2023[8], applied the new concept of window with air supply, and changed the structure of the conventional window to improve the thermal performance. However, changing the window structure is insufficient.

In addition, it is also necessary to take into account the parameters that relate the window to the façade such as the window size [Djamel and Noureddine, 2017[9]], position [Kahsay et al., 2020[10]], and orientation [Kaasaleinen et al., 2020[11]]. In this sense, Amaral et al., 2016[12] considered the number of glazing panes (1-3), size, position, and shadow effect that would improve the window thermal performance in terms of comfort and energy savings; in all cases, single and double glazed had a similar thermal behavior; however, triple glazed provided promising results.

Later, Arici et al., 2020[13] analyzed the effect of the number of panes and the air layer thickness on the overall heat transfer coefficient, U-value; the risk of increasing the U-value in sloped windows can be reduced by using more panes and an optimal air layer thickness. Recently, Rodríguez-Aké et al., 2022[14] reported the first work focused on the thermal performance of a triple-glazed window (TW) under warm climate conditions of Mexico and evaluated the energy saving potential and CO_2 emission compared to single and double glazed windows. Based on the numerical results, the heat flux, energy demand and CO_2 emissions can be reduced by 40 % when triple-glazed is used instead of single-glazed window.

In this study, the potential for energy saving and CO_2 emissions reduction by implementing multi-glazed windows under *Aw* Köppen climate classification is presented. The thermal analysis is carried out based on the numerical modeling of the window heat transfer by mean of the global energy balances method. The temperature and heat flux trends are presented in order to show the window heat transfer rate for the four main orientations. Subsequently, the triple glazed annual thermal performance is presented in order to describe the window orientation advantages and disadvantages.

2. Physical and mathematical model

The physical model, the coordinate system, and the nomenclature used in the numerical solution of multi-glazed windows are shown in Figure 3; the triple glazed window was considered as a representative system. Three semitransparent walls form the TW configuration with a height of Hy=0.80 m and a thickness of $x_{glazing}$=0.006 m; an air-gap b=0.02 m separates each glazing from another. The horizontal walls, top and bottom, are adiabatic.

According to Figure 4, glazing 1 is in contact with the internal temperature, T_{in}=25 °C, while glazing 3 is subjected to external conditions of temperature (T_{out}), wind speed (V_{wind}), and solar radiation (G_{solar}). The heat transfer mechanisms involved in TW are shown in Figure 4a: conduction through semi-transparent walls, natural convection in the encapsulated air, and surface radiation between the vertical walls in both cavities. Conjugate heat transfer comes into play across the boundaries that make up the TW. The normal component of solar radiation strikes the surface of glazing 3; it is reflected, absorbed, and transmitted through the glazing in different proportions, as shown in Figure 4b.

Figure 3 Physical model of a multi-glazed window: TW configuration

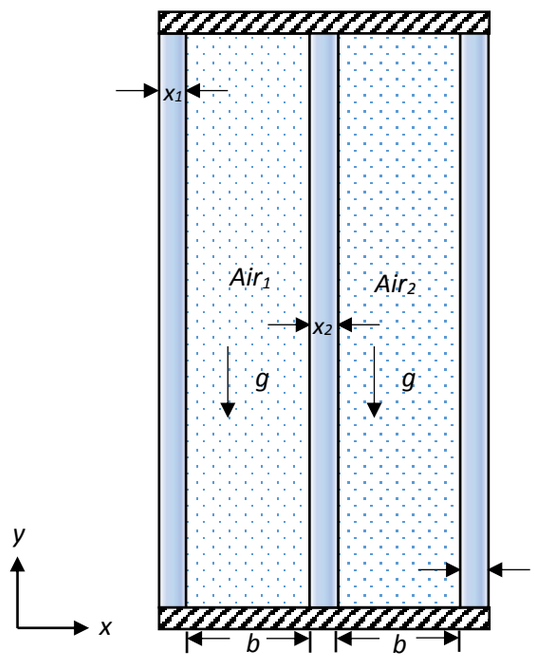

Source: Own Elaboration

The energy absorbed by the semitransparent walls increases the window temperature, so do the radiative and convective heat transfer rate. The value of the heat transfer coefficient by convection between the interior environment and glazing 1 is considered constant, h_{in}=8.3 W/m^2 [ASHRAE Book, 2001[15]]. To determine the value of the convective coefficient between the external environment and the glazing 3 Eq. (1) was used [Zhang et al., 2019[16]]; the external convective coefficient depends on the wind speed.

$$h_{out}^{conv} = 2.8 + 3V_{wind} \tag{1}$$

The emissivity of all glazings is assumed to be constant ε=0.85, and their surfaces are considered opaque, gray, and diffuse to long wave radiation. The thermophysical properties of the glazings were taken from [4], and the optical properties were calculated through the WINDOW[17] software.

Considerations for the mathematical model

- Two-dimensional heat transfer in transient state is considered.
- Due to the dimensions of the window and the difference in temperature that can occur between the glazings, the flow regime is laminar.
- Encapsulated air in DW and TW configurations is considered a Newtonian and incompressible fluid.
- Due to the low moisture content, the air is considered dry; therefore, it is a non-radiatively participating medium.
- The thermophysical and optical properties of glazings are constant.
- On the surface radiative exchange model, the surfaces are considered opaque, diffuse and isothermal.

Figure 4 Conjugate heat transfer in triple-glazed window

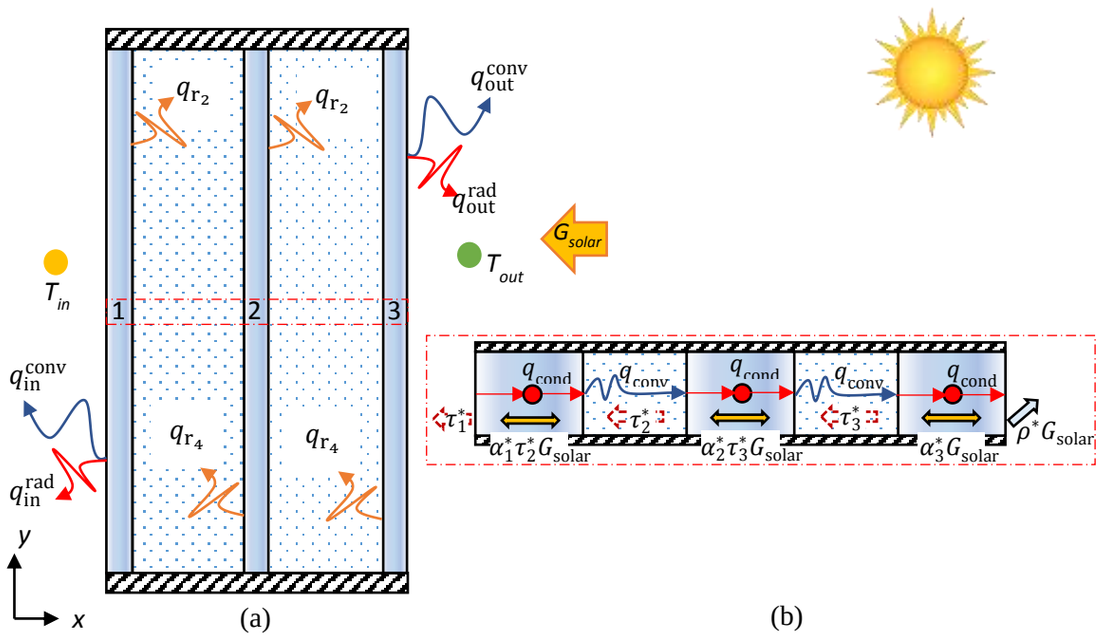

Source: Own Elaboration

In this study, according to Figure 5 the heat flux direction the heat flux direction was assumed from left to right. In order to consider the two-dimensional effect on heat transfer, the three window configurations were divided into multiple sections sections all along the height, as shown in Figure 5a. An energy balance was performed for each section at a point in the center of the glazings. Figure 5b shows the model of thermal resistances with which the heat transfer by conduction (R_{cond}), convection (R_{conv}), and radiation (R_{rad}) in the TW is represented. The value of the conductive thermal resistances for the glazings $\left(R_{glass}^{cond}\right)$ is presented in Eq. (2). As for the encapsulated air, for the encapsulated air, the thermal resistance by convection is represented by Eq. (3).

$$R_{glass}^{cond} = \frac{Hx_{glass}}{2\lambda_{glass}} \tag{2}$$

$$R_{air}^{conv} = \frac{1}{h_{air}^{conv}} \tag{3}$$

Eq. (4) was used to determine the convective heat transfer coefficient for the encapsulated air. This equation relates the Nusselt number (Nu), the air thermal conductivity (λ_{air}), and the characteristic length, L_C; the characteristic height is computed in each section and depends on the position where the energy balance is carried out.

$$h_{air}^{conv} = Nu\frac{\lambda_{air}}{L_C} \tag{4}$$

On the other hand, to determine the Nusselt number, the correlations of Eqs. (5) and (6) were obtained following the methodology reported by Xamán et al., 2005[18].

$$A = 40 \quad \begin{cases} Nu = 6.4411 \times 10^{-16} Ra^2 + 1.9150 \times 10^{-9} Ra + 40 & (5) \\ Ra \leq 6.4 \times 10^7 \\ Nu = 2.8765 \times 10^{-1} Ra^{2.6832^{-1}} & (6) \\ 6.4 \times 10^7 < Ra \leq 6.4 \times 10^{10} \end{cases}$$

The thermal resistances by convection and radiation inside (R_{in}^{conv} and R_{in}^{rad}) and outside (R_{out}^{conv} and R_{out}^{rad}) of the window include the heat transfer coefficients by convection (h^{conv}) and radiation (h^{rad}). Figure 5b shows the thermal conductances C_{g_1}, C_{g_2} and C_{g_3}, which are used to represent the time dependency effect; These include the density (ρ_g), the specific heat (Cp_g), the thickness of each glazing (Hx_g), and the temperature variation over time; the conductances are determined by Eq. (7).

$$C_g = \rho_g Cp_g Hx_g \frac{\partial T_g}{\partial t} \tag{7}$$

Figure 5c shows the heat fluxes resulting from the radiative exchange between surfaces (q_r) and the energy absorbed by the incidence of solar radiation ($\alpha^* G_{solar}$). The radiative heat fluxes, q_{r_2}, and q_{r_4} were calculated by the radiosity-irradiation method (RIM). The Hottel Crossed String method was used to determine the view factors.

Figure 5. Thermal resistances and energy balance in a triple-glazed window

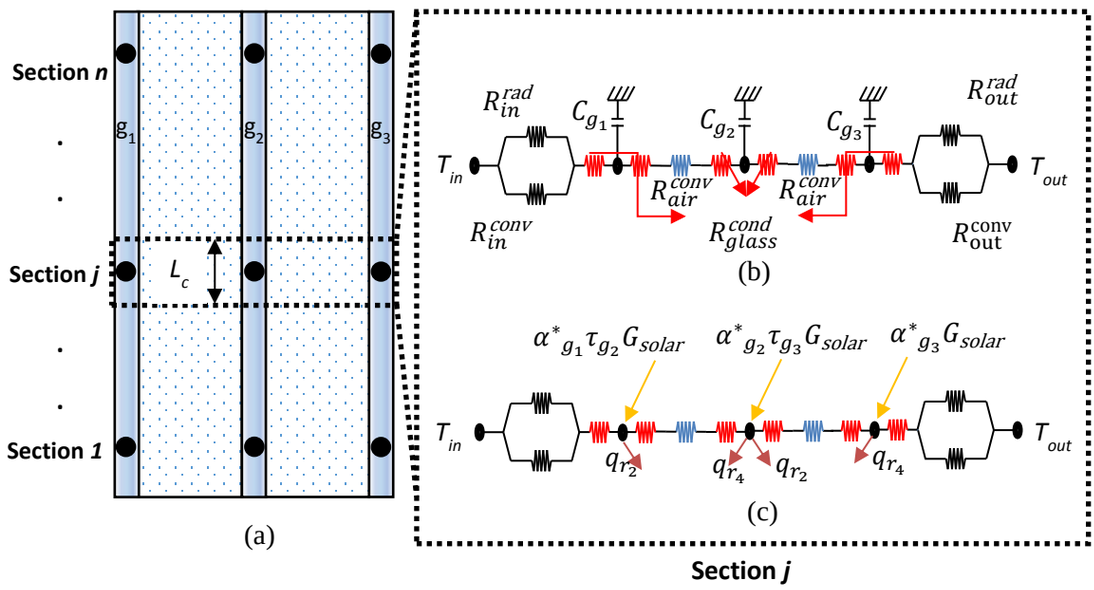

Source: Own Elaboration

An energy balance was performed on the glazings to determine the temperature (see Figure 3a). The point where the energy balance was carried out is called a node. At this point, the energy stored ($q_{storage}$) and exchanged ($q_{in_t} - q_{out}$) in the system is established, as presented in Eq. (8).

$$q_{storage} = q_{in} - q_{out} \tag{8}$$

The energy balances for the configurations of one (SW), two (DW), and three (TW) glazings are presented in equations 9, 10-11, and 12-14, respectively. The total thermal resistances $R_{SPW-g}^{in/out}$, $R_{DPW-g}^{in/out}$ y $R_{DPW-g}^{in/out}$ are defined in Annexes.

SW (9)

$$Cp_{g_1} Hx_{g_1} \frac{\partial T_{g_1}}{\partial t} = \left[\alpha_{g_1}^* G_{solar} + R_{SPW-g_1}^{in}\left(T_{in} - T_{g_1}\right)\right] - \left[R_{SPW-g_1}^{out}\left(T_{g_1} - T_{out}\right)\right] \tag{10}$$

DW – inner glazing (1)

$$\rho_{g_1} Cp_{g_1} Hx_{g_1} \frac{\partial T_{g_1}}{\partial t} = \left[\alpha_{g_1}^* \tau_{g_2} G_{solar} + R_{DPW-g_1}^{int}\left(T_{in} - T_{g_1}\right)\right] - \left[R_{DPW-g_1}^{out}\left(T_{g_1} - T_{g_2}\right) + q_{r_2}\right] \tag{11}$$

DW – outer glazing (2)

$$\rho_{g_2} Cp_{g_2} Hx_{g_2} \frac{\partial T_{g_2}}{\partial t} = \left[\alpha_{g_2}^* G_{solar} + R_{DPW-g_2}^{in}\left(T_{g_1} - T_{g_2}\right)\right] - \left[R_{DPW-g_2}^{out}\left(T_{g_2} - T_{out}\right) + q_{r_4}\right] \tag{12}$$

TW – inner glazing (1)

$$\rho_{g_1} Cp_{g_1} Hx_{g_1} \frac{\partial T_{g_1}}{\partial t} = \left[\alpha_{g_1}^* \tau_{g_2} G_{solar} + R_{TPW-g_1}^{in}\left(T_{in} - T_{g_1}\right)\right] - \left[R_{TPW-g_1}^{out}\left(T_{g_1} - T_{g_2}\right) + q_{r_2}\right] \tag{13}$$

TW – middle glazing (2)

$$\rho_{g_2} Cp_{g_2} Hx_{g_2} \frac{\partial T_{g_2}}{\partial t} = \left[\alpha_{g_2}^* \tau_{g_3} G_{solar} + R_{TPW-g_2}^{in}\left(T_{g_1} - T_{g_2}\right)\right] - \left[R_{TPW-g_2}^{out}\left(T_{g_2} - T_{g_3}\right) + q_{r_2} + q_{r_4}\right] \tag{14}$$

TW – outer glazing (3)

$$\rho_{g_3} Cp_{g_3} Hx_{g_3} \frac{\partial T_{g_3}}{\partial t} = \left[\alpha_{g_3}^* G_{solar} + R_{TPW-g_3}^{in}\left(T_{g_2} - T_{g_3}\right)\right] - \left[R_{TPW-g_3}^{out}\left(T_{g_3} - T_{out}\right) + q_{r_4}\right]$$

3. Numerical solution methodology

In this section, the implemented numerical solution process implemented to determine the temperature in the glazing through equations 9-14 is presented.

The numerical solution flowchart is presented in Figure 6. The numerical code was developed in FORTRAN; an implicit scheme was used to discretize the transient term. As a first step, the dimensions of the system and the modeling time must be entered; from these parameters, the nodes are generated (step 1), and the climatic variables are calculated (step 2), respectively.

Next, the thermophysical properties of air and the convective heat transfer coefficients are calculated (step 3). In step 4, the Jacobi method is applied to solve the equations, and the temperature is obtained. Steps 3 and 4 are repeated until *j=Ny*, according to the number of sections established for the solution. Once this process is complete, a convergence criterion of $1.0E10^{-10}$ must be satisfied. If this criterion is true, the results of each time step are stored and the process starts again from step 2 for the next time step, $t = t + \Delta t$.

Table 1 Results of time step selection

Δt	$T_{g_1}^{average}$ (°C)	Error (%)	q_{in} (W/m^2)	Error (%)
1	31.07	--	82.37	--
3	31.07	0.01	82.35	0.03
5	31.07	0.01	82.32	0.03
10	31.07	0.02	82.25	0.08
15	31.06	0.02	82.18	0.08

Source: Own Elaboration

A time mesh independence study was performed to determine the appropriate time step for modeling, Δt= 1, 3, 5, 10 y 15 s; the number of sections was set at 40. The results of the average temperature and the heat flux to the interior (by convection and radiation) for the TW are shown in Table 1; these results correspond to the hour with the highest solar radiation (952 W/m^2) during the warmest day in Mérida, Yucatán. The difference between the results with different time steps was less than 1 %, so an intermediate time step of 5 s was chosen.

4. Results

The numerical modeling of the three glazing configuration: single (SW), double (DW), and triple (TW) were carried out for the four main orientations, north, south, east and west, under the warm weather conditions of Mérida, Yucatán. The modeling was carried out for the warmest day (in July) and the coldest day (in January) of 2018; the days were chosen based on the outside temperature. The weather data (outside temperature, wind speed and solar radiation) were provided by the National Water Commission (CONAGUA by the acronym in Spanish- MEXICO).

Table 2 Weather data for the warmest and coldest days

Day	Highest temperature (°C)	Lowest temperature (°C)	Solar radiation (W/m^2)			
			North	South	East	West
Warmest	40.8	26.1	366.4	197.6	952.2	595.5
Coldest	22.6	15.1	190.7	270.8	190.4	270.3

Source: National Water Commission (CONAGUA) and National Meteorological Service in Mexico

According to the Köppen climate classification, Mérida has an *Aw* climate, warm tropical with dry winters and humid summers. The highest and lowest values of the outside temperature and the highest value of solar radiation for the orientations described above, for the warmest and coldest days of the year are presented in Table 2. For the coldest day, the values of solar radiation on the north and east surfaces are similar between both, so are the values of solar radiation on the south and west oriented surface. Therefore, the thermal evaluation for the coldest day was carried out only for the north and south orientations.

Figure 6 Flowchart of numerical solution methodology

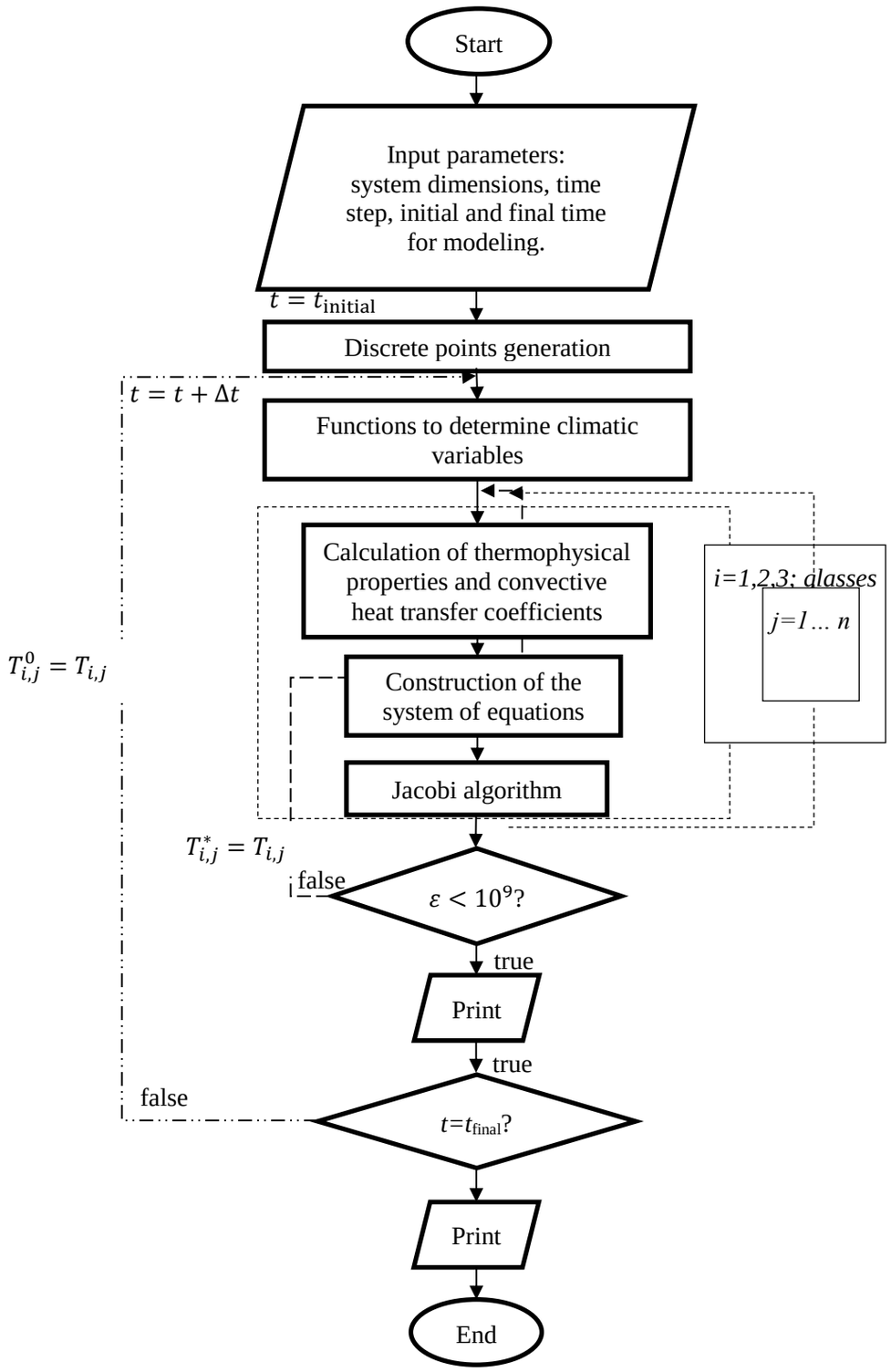

Source: Own Elaboration

4.1 Effect of the panes number on the window thermal performance

For the warmest day, Graphic 1 shows that the average internal surface temperature of glazing 1 ($T_{s,in}^{ave}$) of the triple-glazed (TW) configuration remains below the outside temperature, as well as the temperature of the single (SW) and double (DW) glazed configurations throughout the day. However, the increase in solar radiation from 06:00 h to 08:00 h, causes and increment of $T_{s,in}^{ave}$ on the north oriented surface, where the $T_{s,in}^{ave}$ of the SW and DW configurations exceed the outside temperature by 1 °C during that period.

On the other hand, on the south orientation the most noticeable differences among the configurations occur from 10:00 h to 16:00 h, with a continuous interval of high values of solar radiation and outside temperature; during this period the $T_{s,in}^{ave}$ of the TW configurations remains between 6 °C to 9.5 °C below the outside temperature and 1 °C to 3.5 °C below the $T_{s,in}^{ave}$ of the SW configuration. At 14:00 h in the north and south orientation, the highest temperature of the TW is 31.3 °C, while the highest temperature recorded by the SW and DW configurations is 34.4 °C and 32.5 °C, respectively.

Graphic 1 Average internal surface temperature trend on the warmest day

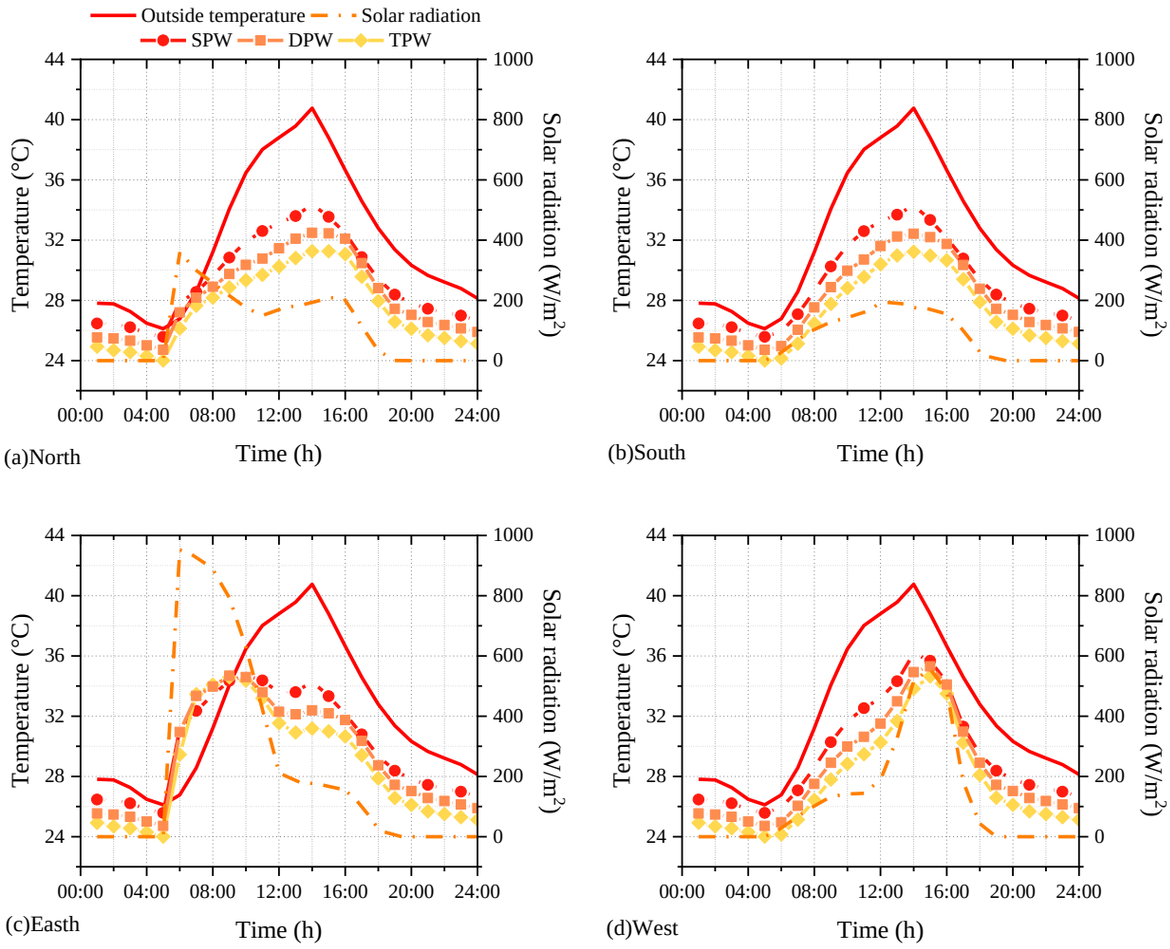

Source: Own Elaboration

On the east and west orientations, Graphic 1c and 1d show that there is an increase of the $T_{s,in}^{ave}$ during the period in which highest peaks of solar radiation occur on both orientations. On the east orientation (Graphic 1c) it is shown that the $T_{s,in}^{ave}$ for the three configurations reaches the highest values from 06:00 h to 12:00 h due to solar radiation with a slight decrease right after 12:00 h in order to raise again, now caused by the increase on the outside temperature and solar radiation values close to 200 W/m^2. However, from 12:00 h to 16:00 h the temperature increases in multiple glazed windows and presents a similar trend to the $T_{s,in}^{ave}$ of the north and south orientations, during this period. On the other hand, the highest temperature values in the three configurations are presented on the west orientation: 36.2 °C, 34.9 °C and 33.8 °C for SW, DW and TW, respectively, at 14:00 h, when solar radiation and the outdoor temperature register the highest values, 595.5 W/m^2 and 40.8 °C, respectively. In this orientation, the temperature in the three window configurations remains 2 °C above the highest temperature recorded in the other orientations at 14:00 h.

For the coldest day, Graphic 2 shows that the difference for $T_{s,in}^{ave}$ among configurations for all orientations is approximately 0.03 °C. On the other hand, the $T_{s,in}^{ave}$ of the DW and TW configurations stayed above the outside temperature all along the day, unlike the $T_{s,in}^{ave}$ of the SW configuration which falls 2 °C below the outside temperature by the end of the day, and 1 °C below the $T_{s,in}^{ave}$ of the DW and TW configurations. The lowest outdoor temperature value occurred at 05:00 h, the $T_{s,in}^{ave}$ of the SW and TW remained 4.9 °C above the outdoor temperature, while the DW configuration was also 5.2 °C above.

The total heat flux, $q_{total\text{-}in}$, was determined to quantify the heat transfer through the window; the total heat flux is the product of the contributions by convection, radiation and the heat flux transmitted due to the incidence of solar radiation. When $T_{s,in}^{average} > T_{in}$, $q_{total\text{-}in}$ the value is positive, and it indicates that the window gains energy from the outside environment and transports it towards the inside. On the other hand, if the $q_{total\text{-}in}$ values are negative, it is an indication that energy is transferred from the interior environment towards the outside through the window, because $T_{s,in}^{average} < T_{in}$. Consequently, the window releases energy (loses energy) to the outside environment.

Graphic 2 Average internal surface temperature trend on the coldest day

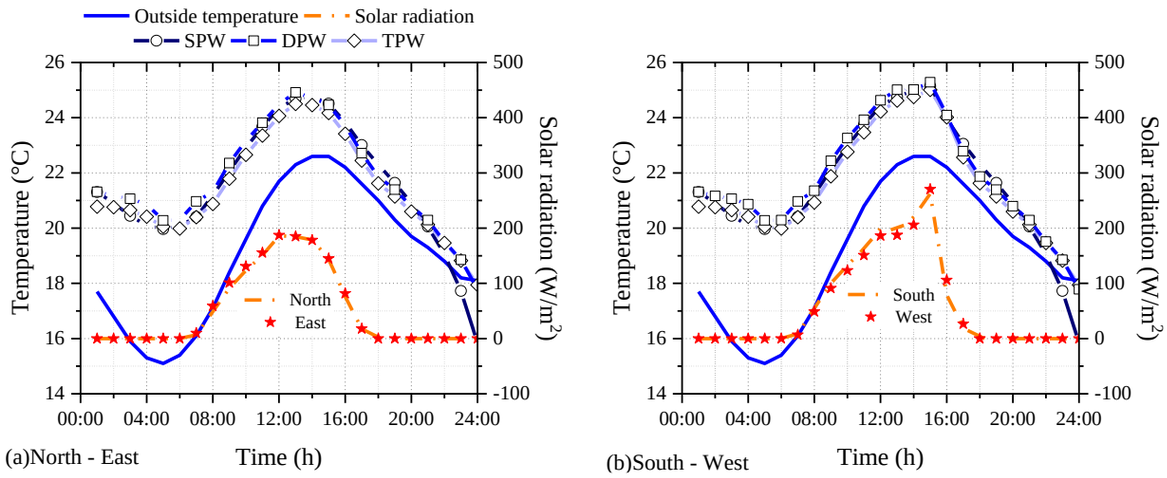

Source: Own Elaboration

Graphic 3. Heat flux trend on the warmest day

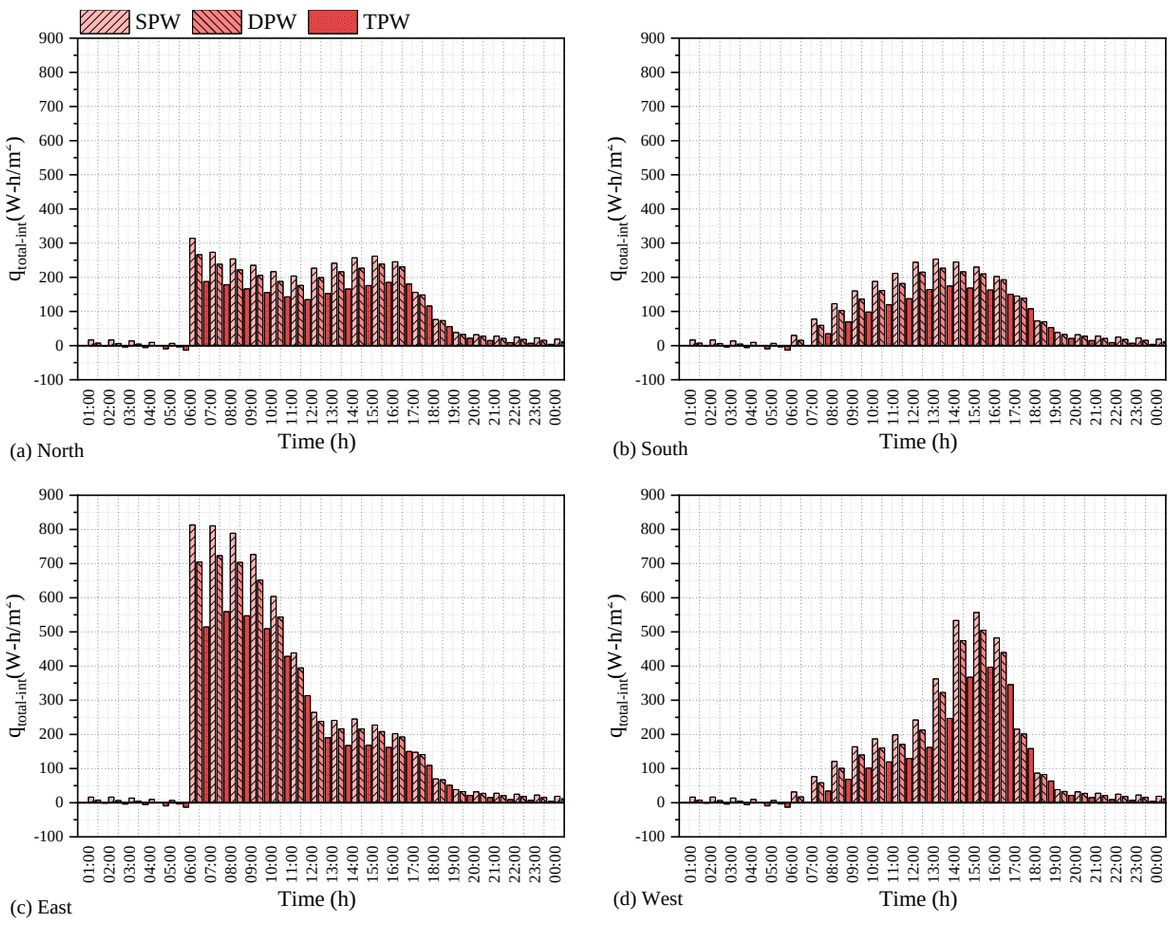

Source: Own Elaboration

For the warmest day, Graphic 3 shows that the single glazing (SW) and double glazing (DW) configurations reach the highest values of $q_{total\text{-}in}$ for all orientations, even at times in absence of solar radiation. The east orientation $q_{total\text{-}in}$ registers the highest values of $q_{total\text{-}in}$ at 06:00 h, with 812.8 W/m^2, 704.5 W/m^2, and 514.4 W/m^2 for SW, DW and TW, respectively. At this time, solar radiation reaches the highest value (952.2 W/m^2), causing an increase in the transmitted heat flux, which represents the greatest contribution of $q_{total\text{-}in}$.

For the north orientation, the TW reaches the highest value (187.4 W/m^2) also at 06:00 h, while for the south and west orientations it occurs at 14:00 h with values of: 162.9 W/m^2 and 396.7 W/m^2, respectively. In the east orientation, the one with the highest values of solar radiation (specifically at 06:00 h), with respect to the single glazing configuration, the TW reduces energy gains up to 36.7%, while the DW reduces them by 13.3 %. Throughout the day the heat flux values are positive, this is because the outside temperature is higher than the 25 °C inside temperature, so the window continually gains energy, these gains increase as solar radiation does.

For the coldest day, Graphic 4 shows that the heat flux through the window presents positive and negative values, that is, the window gains and loses energy throughout the day, unlike the warmest day, in which the window gains energy all day long (except for the hours 00:00 h to 05:00 h). On the coldest day, from 09:00 h to 16:00 h, the values of $q_{total\text{-}in}$ are positive, during this period the highest values of $q_{total\text{-}in}$ that correspond to the TW are: 81.3 W/m^2 and 125.4 W/m^2 on the north and south surfaces, respectively.

On the other hand, in absence of solar radiation, the variables that define the thermal behavior of the window are the outside temperature and the wind speed. These variables do not depend on the orientation; therefore, similar energy losses occur in the four orientations: -101.4 W/m^2, -95.4 W/m^2,and -93.3 W/m^2 for SW, DW and TW, respectively. Regarding the SW configuration, the TW reduces the energy losses through the window by 8 %, while the DW reduces them by 5.9 %.

Graphic 4 Heat flux, three glazed types, all orientation on the coldest day

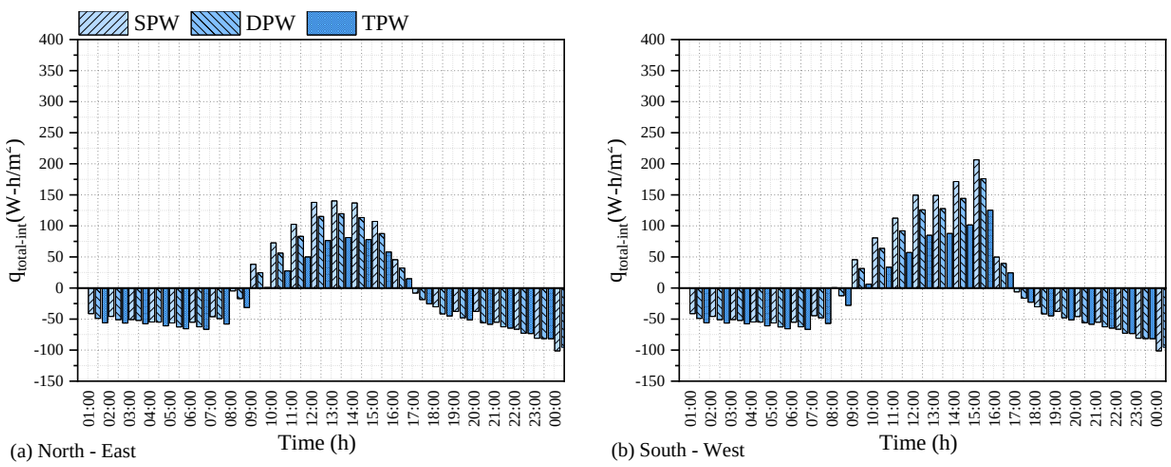

Source: Own Elaboration

Table 3 presents the results of the numerical integration of $q_{total\text{-}in}$ per hour during the warmest and coldest day of the year for the three configurations and the four orientations, this integration represents the thermal energy load of the window. For the warmest day, the lowest energy gain of all the configurations is registered on the south orientation, while the highest is presented on the east orientation; this is largely due to the solar radiation that hits on both orientations. However, on all orientations, the TW configuration presents the lowest energy gains: 2.08 kWhm^{-2}, 1.53 kWhm^{-2}, 3.96 kWhm^{-2}, and 2.28 kWhm^{-2} on the north, south, east and west orientations, respectively. The TW configuration reduces the energy gain to the building by 35.9 % y 13.6 % with respect to the SW and DW configurations, respectively.

Table 3 Average heat flux, three glazed types, all orientations

Orientation	$\int_{time_{initial}}^{time_{final}} \lvert q_{total\text{-}in}(t) \rvert \, dt$, (kWhm^{-2})					
	Warmest day				Coldest day	
	SW	DW	TW		SW	DW	TW
North	3.17	2.77	2.08		1.48	1.44	1.26
South	2.39	2.06	1.53		1.67	1.60	1.39
East	5.79	5.14	3.96		1.51	1.45	1.27
West	3.47	3.02	2.28		1.64	1.57	1.36

Source: Own Elaboration

On the other hand, for the coldest day the values of solar radiation are similar, due to this the energy gain in all orientations is similar. However, there is a significant difference between configurations. The north orientation, followed by the east, present the lowest energy gain, while the south orientation registers the highest: 1.67 kWhm^{-2}, 1.60 kWhm^{-2}, and 1.39 kWhm^{-2} for SW, DW and TW, respectively. For the south orientation, the TW configuration reduces the energy gain by 16.9 % with respect to SW, while the DW reduces it by 4.3 %.

4.2 Annual Thermal Evaluation - Triple Glazed Window (TW)

The results obtained for the warmest and coldest day of the year showed that multiple glazings, specifically the triple glazing (TW) configuration. However, evaluating only two days of the year provides little revealing data to support that the triple glazing configuration has favorable results throughout the year. Due to this, the thermal analysis of the window with the TW configuration was carried out during the warmest and coldest day of each month of an entire year. For the annual evaluation, the window is also considered in different orientations.

Table 4 The lowest and highest values of outside temperature per month

Month	Warmest day		Coldest day	
	T_{out}^{max} (°C)	T_{out}^{min} (°C)	T_{out}^{max} (°C)	T_{out}^{min} (°C)
January	33.4	21.7	22.6	15.1
February	36.9	22.0	32.0	16.9
March	39.8	23.4	35.5	18.2
April	40.8	23.4	29.3	17.7
May	39.4	25.2	37.4	22.3
June	38.9	24.4	33.8	23.3
July	40.8	26.1	35.7	23.8
August	37.4	25.5	38	25.5
September	36.9	23.8	36.2	22.0
October	36.6	22.9	35.0	20.3
November	35.3	22.8	29.0	15.7
December	35.8	21.7	28.4	11.2

Source: Own Elaboration

Since the outside temperature does not depend on the orientation, the highest and lowest values are the same for all four orientations, these are presented in Table 3 for the warmest and coldest days of the year. The highest temperature all along the year occurs in two months: April and July, with a value of 40.8 °C. However, on the warmest day in April the lowest temperature is 23.4 °C, approximately 3 °C below the lowest temperature recorded on the warmest day in July (26.1 °C). On the other hand, on the coldest days, the lowest temperature value occurs in December (11.2 °C). However, unlike January, the temperature interval is wider and reaches up to 28.4 °C, while in January the outside temperature only reaches 22.6 °C.

The solar radiation values depend on orientation; the lowest values occur on the north orientation, during autumn and winter. On the other hand, the south orientation has a longer exposure time to direct solar radiation of approximately 12 continuous hours and the values of solar radiation during autumn and winter are similar to those presented for the east and west orientations. However, these orientations only receive direct solar radiation for 6 hours, on the first and last hours of the sun.

Graphics 5-8 show the results of temperature and total heat flux of the window with the TW configuration with respect to the outside temperature and solar radiation that were recorded on the warmest and coldest days of the year (24 days) in different orientations.

The north orientation only receives direct solar radiation in spring and summer, due to this an increase in solar radiation values is recorded during these seasons, specifically in the period from May to July (see Graphic 5). The highest value of solar radiation occurs in July (360.8 W/m^2) for the warmest days and in June (376.8 W/m^2) for the coldest days. In autumn and winter, radiation values are very low, and the highest values barely reach 136.6 W/m^2 and 132.3 W/m^2 in December for the warmest days and in February for the coldest days, respectively.

On the warmest days (Graphic 5a) the interval of the highest $T_{s,in}^{ave}$ is 28.2 °C to 31.4 °C, the highest value was recorded in May, when the outside temperature reached 39.4 °C and solar radiation was 232.8 W/m^2. On the other hand, the highest total heat flux ($q_{total\text{-}in}$) is in the interval of 112 W/m^2 to 195.4 W/m^2. The increase in solar radiation from May to July favors an increase in $T_{s,in}^{ave}$ and in $q_{total\text{-}in}$, since the highest values of both variables are recorded in these months. Except for these months, the highest $q_{\text{total-int}}$ through the window does not exceed 150 W/m^2. For the coldest days (Graphic 5b), the highest outside temperature and the highest $T_{s,int}^{ave}$ were recorded in August: 38 °C and 30.3 °C, respectively. For the coldest day in August, the highest solar radiation is 192.7 W/m^2, while the $q_{total\text{-}in}$ is 157.9 W/m^2. For the coldest days, the interval of the highest $T_{s,in}^{ave}$ is 24.5 °C to 30.3 °C, while that of the highest $q_{total\text{-}in}$ is 69 W/m^2 to 201.5 W/m^2. The highest value of $q_{total\text{-}in}$ coincides with the day in which the highest solar radiation occurs, which for these days is in June.

Graphic 5 Triple-glazed annual thermal performance (a) the warmest period and (b) the coldest period, north orientation

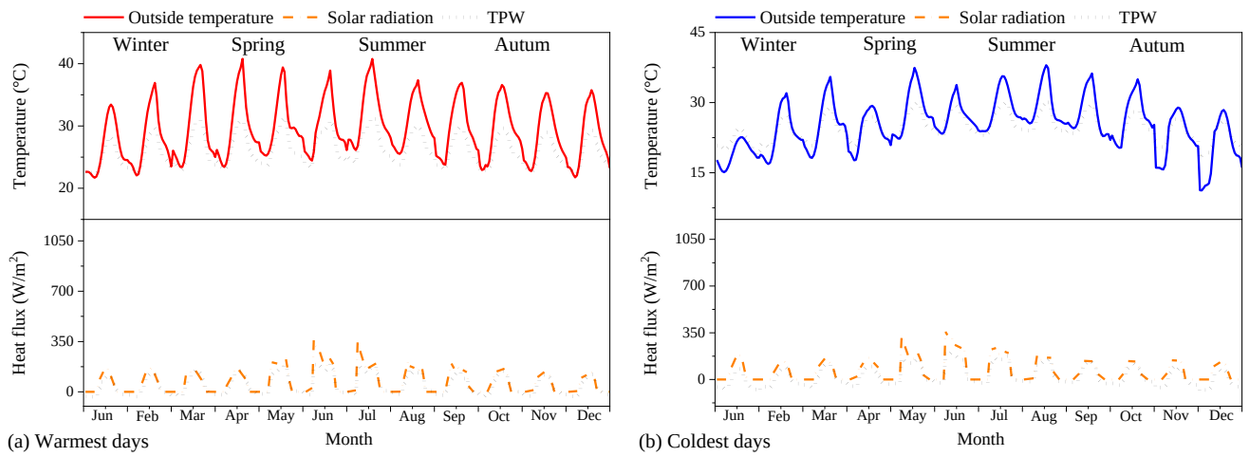

Source: Own Elaboration

Unlike the north orientation, direct solar radiation affects the south orientation all year round, especially during autumn and winter (see Graphic 6), due to this an increase in solar radiation values is generated from September to February. On the warmest days, the highest values of solar radiation are between 174.2 W/m^2 to 893.1 W/m^2, while on the coldest days these values are between 159.2 W/m^2 to 915 W/m^2. The lowest values of solar radiation are recorded in spring and summer: in June for the warmest days and in July for the coldest days.

For the warmest days, Graphic 6a shows that the highest values of $T_{s,in}^{ave}$ and $q_{total\text{-}in}$ are strongly affected by the behavior of solar radiation, the outside temperature is neglected. In January, the highest value of $T_{s,in}^{ave}$ is 34.3 °C, approximately 1 °C above the outside temperature recorded in that month. The increase in $T_{s,in}^{ave}$ and solar radiation lead to an increase in the total heat flux, due to this the highest $q_{total\text{-}in}$ interval on the warmest days is: 138.5 W/m^2 to 539.2 W/ m^2. With respect to the highest total heat flux recorded on the north orientation, the highest $q_{total\text{-}in}$ on the south is above 343.8 W/m^2. For the coldest days, Graphic 6b shows that the solar radiation also leads to an increase in the window temperature, especially in February, November and December when the $T_{s,in}^{ave}$ exceeds the outside temperature by up to 3.9 °C.

The highest $T_{s,in}^{ave}$ values fall between 25 °C to 33.4 °C, while the highest $q_{total\text{-}in}$ values fall between 125.4 W/m^2 to 540.5 W/m^2. Because in January the difference between the interior temperature and $T_{s,in}^{ave}$ is minimal, there is no heat transfer by convection and radiation, so the main contribution of $q_{total\text{-}in}$ is radiation solar energy that falls on the window in different orientations.

Graphic 6 Triple-glazed annual thermal performance (a) the warmest period and (b) the coldest period, south orientation

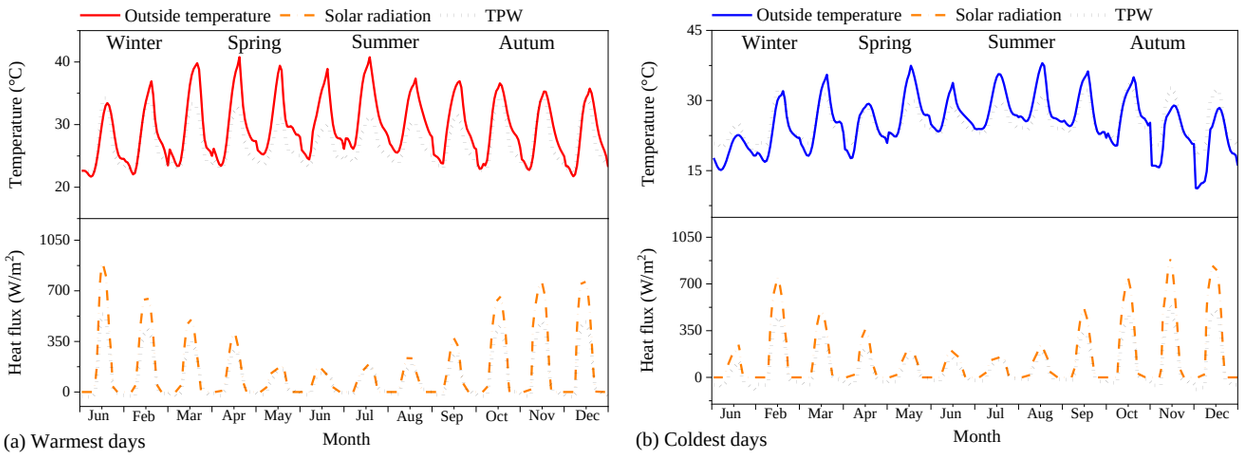

Source: Own Elaboration

On the warmest and coldest days, the lowest energy gains (positive heat flux) through the window were recorded from May to August, months in which solar radiation is less than 200 W/m^2, despite the fact that in these months, the highest outdoor temperature values between 37.4 °C to 40.8 °C on the warmest days and 36.7 °C to 38 °C on the coldest days.

The sun trajectory begins in the east orientation, from approximately 06:00 h to 12:00 h, time when the highest values of solar radiation are recorded, even more so in spring and autumn, seasons in which the sun does not tilt to the north or south. On the warmest days the highest solar radiation is between 455.4 W/m^2 to 1034.8 W/m^2, while on the coldest days is between 187.2 W/m^2 to 1008.7 W/m^2, on both days the lowest values occur in January and the highest in November. As shown in Graphic 7, the increase in solar radiation during the first hours of the day causes an increase in $T_{s,in}^{ave}$ before the outside temperature reaches the highest value on the warmest and the coldest days.

On the warmest days (Graphic 7a), the highest $T_{s,in}^{ave}$ value is between 28.3 °C to 34.6 °C, while the highest $q_{total\text{-}in}$ value is between 246.3 W/m^2 to 580.1 W/m^2. The highest $T_{s,in}^{ave}$ is recorded in July and is 6 °C below the highest outside temperature. While the $q_{total\text{-}in}$ occurs in November when solar radiation reaches 1034.8 W/m^2. On the coldest days (Graphic 7b), from November to January the $T_{s,in}^{ave}$ exceeds the outside temperature by up to 3 °C, while in the other months it remains up to 5 °C below. Although in November and December, the outside temperature barely reaches 28.9 °C, the solar radiation exceeds 950 W/m^2, so the window absorbs energy and increase the temperature, which is why the $T_{s,in}^{ave}$ reaches up to 32 °C . On the other hand, the highest $q_{total\text{-}in}$ is between 81.6 W/m^2 to 573.5 W/m^2, the highest value occurs in May due to the combination of high values of solar radiation (996 W/m^2) and the outside temperature (37.4 °C).

Unlike the north and south orientations, for the east orientation the results between months are not far from each other since the solar radiation in this orientation does not present a significant variation with the change of seasons.

Graphic 7 Triple-glazed annual thermal performance (a) the warmest period and (b) the coldest period, east orientation

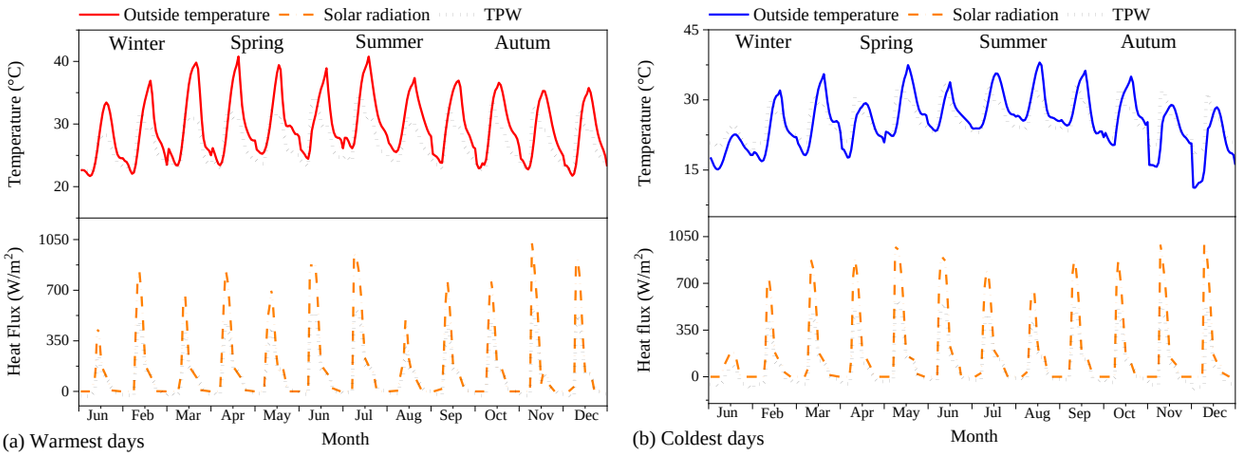

Source: Own Elaboration

For the west orientation, Graphic 8 shows that the solar radiation values rise after noon and until sunset, which occurs at approximately 18:00 h. On the warmest days, the interval of the highest solar radiation value is between 459.7 W/m^2 to 1098.9 W/m^2, while on the coldest it is 270.3 W/m^2 to 832 W/m^2. On the warmest days, the highest value is recorded in October and the lowest in December, while on the coldest days the highest is in April and the lowest in January. For this orientation, the highest value of solar radiation and outside temperature coincide in the hour, this causes the $T_{s,in}^{ave}$ and the highest outside temperature also to coincide. However, when this does not happen, a gap between both reference lines can be observed, as it occurs on the warmest day in October (see Graphic 8a).

On the warmest days, the interval of the highest $T_{s,in}^{ave}$ is 32 °C to 36.5 °C, while the interval of the highest $q_{total\text{-}in}$ is 314.2 W/m^2 to 679.1 W/m^2. The highest values of both variables are recorded in October, because on this day the solar radiation reaches 1099 W/m^2. On the other hand, on the coldest days the highest $T_{s,int}^{ave}$ is recorded in March when the outside temperature is 35.5 °C and solar radiation is 735.2 W/m^2. However, the highest $q_{total\text{-}in}$ occurs in April, although the outside temperature is 6 °C lower than in March, due to the fact that solar radiation is 832 W/m^2. These days the highest $T_{s,in}^{ave}$ interval is between 24.9 °C to 34.3 °C, while the highest $q_{total\text{-}in}$ interval is 128.2 W/m^2 to 487.6 W/m^2.

Graphic 8 Triple-glazed annual thermal performance (a) the warmest period and (b) the coldest period, west orientation

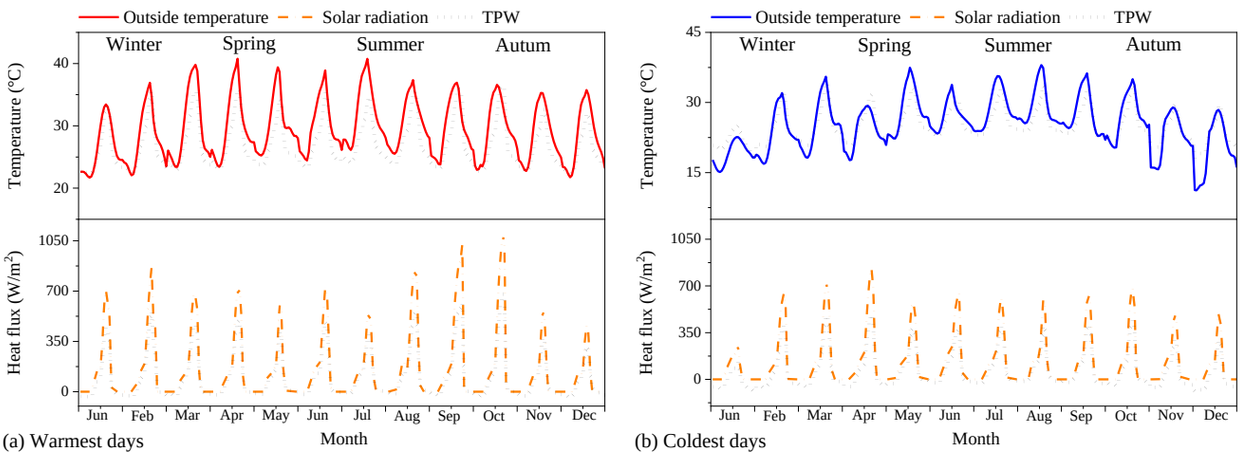

Source: Own Elaboration

In the absence of solar radiation, the effect of the window orientation is negligible, because the variables that define the thermal behavior of the window are: outside temperature and wind speed. In general, during the early morning the outside temperature remains below the inside temperature of 25 °C, this causes the surface temperature of the window to remain very close to the inside temperature and the heat flux is negative. Table 5 shows the lowest values of $T_{s,in}^{ave}$ and $q_{total\text{-}in}$; on the warmest days the interval of the lowest $T_{s,in}^{ave}$ is 22.3 °C to 24 °C, while on the coldest days it is 17.9 °C to 23.7 °C. In winter, specifically in December, the lowest $T_{s,in}^{ave}$ remains up to 6 °C above the lowest outside temperature recorded in that month. Regarding $q_{total\text{-}in}$, for both days the lowest values recorded in January are: -35.8 W/m^2 and -93.33 W/m^2 for the warmest and coldest days, respectively. The heat flux is negative, because the energy is transferred from the interior environment to the window, since the interior temperature is greater than $T_{s,in}^{ave}$.

Table 5 The lowest temperature and heat flux values per month, triple-glazed window

Month	Warmest days		Coldest days	
	$T_{s,in}^{ave}$ (°C)	$q_{total\text{-}in}$ (W/m^2)	$T_{s,in}^{ave}$ (°C)	$q_{total\text{-}in}$ (W/m^2)
January	22.3	-35.8	17.9	-93.3
February	22.5	-34.0	20.6	-59.0
March	23.0	-26.7	20.8	-55.6
April	23.0	-26.4	20.8	-56.0
May	23.6	-18.2	22.5	-33.3
June	23.3	-23.1	23.0	-27.1
July	24.0	-13.3	23.0	-26.0
August	23.8	-16.6	23.7	-16.9
September	22.9	-26.3	22.6	-31.9
October	22.7	-30.4	21.8	-42.7
November	22.7	-30.5	20.3	-63.0
December	22.3	-35.4	18.0	-91.7

Source: Own Elaboration

4.3 Energy demand and CO_2 emissions of Triple-glazed window

Graphic 9 shows the energy gains towards the building due to the use of the TW configuration in different orientations on the warmest and coldest days of the year. On the warmest days the energy gain interval on the north orientation is 1.01 kWhm^{-2} to 2.21 kWhm^{-2}, on the south it is 1.31 kWhm^{-2} to 3.93 kWhm^{-2}, on the east 1.40 kWhm^{-2} to 3.96 kWhm^{-2} and on the west 1.66 kWhm^{-2} to 3.65 kWh^{-2}. While on the coldest days the intervals are: 1.11 kWhm^{-2} to 2.18 kWhm^{-2} on the north, 1.27 kWhm^{-2} to 4.50 kWhm^{-2} on the south, 1.27 kWhm^{-2} to 3.84 kWhm^{-2} on the east, and 1.36 kWhm^{-2} to 2.83 kWhm^{-2} on the west.

Graphic 9 Annual energy demand of triple-glazed window

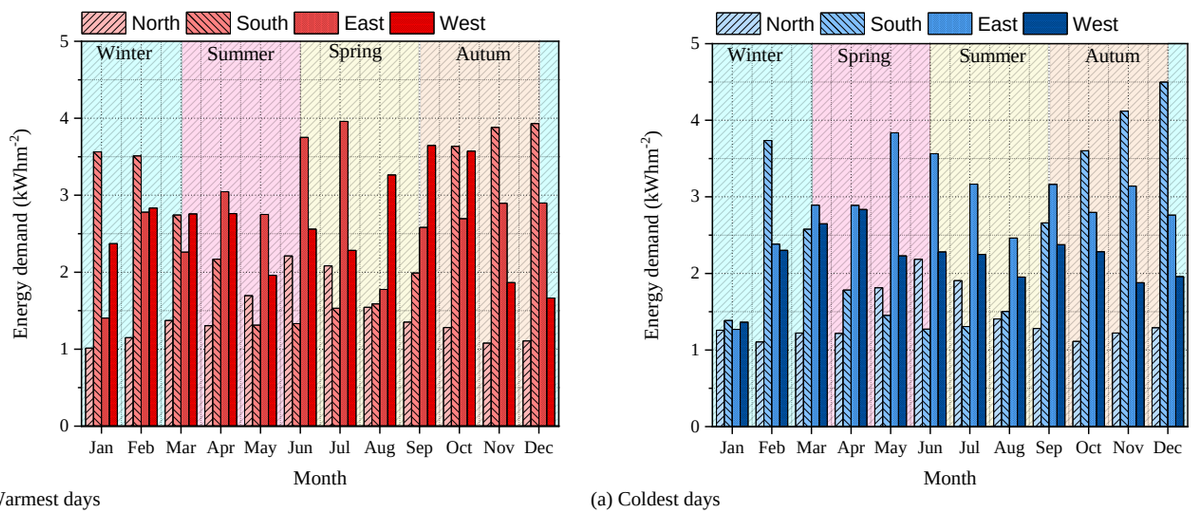

(a) Warmest days

(a) Coldest days

Source: Own Elaboration

The greatest energy gain occurs in the months in which solar radiation registers the highest values on each orientation. For example, on the warmest days (Graphic 9a) the solar radiation on the south orientation reaches the highest values in autumn and winter; from October to February, the energy gain was in the interval 3.51 $kWhm^{-2}$ to 3.88 $kWhm^{-2}$, providing this period the highest values out of all the orientations. On the north orientation, the greatest energy gain occurs from May to July in the interval of 1.70 $kWhm^{-2}$ to 2.21 $kWhm^{-2}$, however, these values remain below the results on the east and west orientations. On the east orientation, the greatest energy gain was obtained from April to July with values ranging from 2.75 $kWhm^{-2}$ to 3.96 $kWhm^{-2}$. While on the west orientation, the greatest energy gain occurred in August (3.26 $kWhm^{-2}$) and September (3.57 $kWhm^{-2}$).

On the warmest days, the east orientation shows the greatest energy gain, followed by the west, south, and north orientations. On the other hand, on the coldest days, the increase in solar radiation on the south orientation in February and from October to December causes an increase in energy gain (see Graphic 9b), even when the outside temperature decreases in these months. During this period, the energy gain on the south orientation is greater than the other orientations; in December, the highest recorded value of energy gain is: 4.50 $kWhm^{-2}$. On the other hand, the north orientation, for the warmest days, registers the lowest energy gain, except in the period from May to July (1.81 $kWhm^{-2}$ to 2.18 $kWhm^{-2}$). From March to September on the east orientation, the energy gains are in the interval of 2.46 to 3.84 $kWhm^{-2}$. On the coldest days, the energy gain in the west orientation is not greater than within other orientations: 1.36 $kWhm^{-2}$ to 2.83 $kWhm^{-2}$; the highest value occurs in April and the lowest in January.

Table 6 shows the annual atmospheric CO_2 emissions due to the heat flux through the window with the triple-glazed window. The conversion of energy into CO_2 emissions was based on the 2021 electricity emission factor of 0.423 tCO_2e/MWh that was established by the Ministry of the Environment and Natural Resources of Mexico to calculate the indirect emission of greenhouse gases from the consumption of electricity.

Table 6 CO_2 emissions per year, triple-glazed window in all orientations

	Orientation			
	North	**South**	**East**	**West**
CO_2 emissions ($kgCO_2em^{-2}$)	217.08	387.56	425.90	367.36

Source: Own Elaboration

Annexes

Nomenclature

A	aspect ratio
b	air layer thickness, (m)
C_P	specific heat, (J kg K^{-1})
G	solar radiation, (W m^{-2})
H_y	height of the window, (m)
H_x	glazing thickness, (m)
L_C	characteristic length, (m)
Nu	Nusselt number
q	heat flux, (W/m^2)
Ra	Rayleigh number
T	temperature, (°C)
t	time, (s)
V_{air}	wind speed, (m/s)
x, y	cartesian coordinates

greek

α^*	absortance
Δt	step time, (s)
ε	emittance
λ	thermal conductivity, (W m^{-1} K^{-1})
ρ	density, (kg m^{-3})
ρ^*	reflectance
σ	Stefan – Boltzman's constant, (5.67×10^{-8} W m^{-2} K^{-4})
τ^*	transmittance

subscripts

cond	conductive
conv	convective
out	outside
g	glazing
in	interior
rad	radiative
s, in	internal surface

abbreviations

SW	single glazing window
DW	double glazing window
TW	triple glazing window

The total thermal resistances $R_{SPW-g}^{in/out}$, $R_{DPW-g}^{in/out}$ y $R_{DPW-g}^{in/out}$ are defined as:

$$R_{SPW-g_1}^{in} = R_{DPW-g_1}^{in} = R_{TPW-g_1}^{in} = \left(\frac{1}{h_{in}^{conv} + h_{in}^{rad}} + \frac{Hx_g}{2\lambda_g}\right)^{-1} \tag{17}$$

$$R_{SPW-g_1}^{out} = R_{DPW-g_2}^{out} = R_{TPW-g_3}^{out} = \left(\frac{Hx_g}{2\lambda_g} + \frac{1}{h_{out}^{conv} + h_{out}^{rad}}\right)^{-1} \tag{18}$$

$$R_{DPW-g_1}^{out} = R_{DPW-g_2}^{in} = R_{TPW-g_1}^{out} = R_{TPW-g_2}^{in} = \left(\frac{Hx_g}{2\lambda_g} + \frac{1}{h_{air_1}^{conv}} + \frac{Hx_g}{2\lambda_g}\right)^{-1} \tag{19}$$

$$R_{TPW-g_2}^{out} = R_{TPW-g_3}^{in} = \left(\frac{Hx_g}{2\lambda_g} + \frac{1}{h_{air_2}^{conv}} + \frac{Hx_g}{2\lambda_g}\right)^{-1} \tag{20}$$

Acknowledgment

LÓPEZ-SALAZAR Samanta acknowledge to the National Council of Humanities, Sciences and Technologies (CONAHCYT) for the financial support given through her doctorate scholarship program (grant number 789202).

LIMA-TÉLLEZ Thania Guadalupe acknowledge to the National Council of Humanities, Sciences and Technologies (CONAHCYT) for the financial support given through her doctorate scholarship program (grant number 768967).

Conclusions

In this work, the effect of multi-glazed on a window thermal performance under *Aw* Köppen climate classification was analyzed. Based on the numerical modeling of the conjugate heat transfer, on a two-dimensional window in transient state, the following is concluded:

– On the warmest day of the year, the surface temperature of the TW configuration remained 3.5 and 9.5 °C below the temperature of the SW configuration and the outside temperature, respectively. The DW configuration reduces the window temperature by 8.3 °C from outside temperature. On the other hand, on the coldest day, the TW remained up to 4.9 °C above the lowest outside temperature value.

– In terms of energy gain/loss, on the warmest day the DW and TW configurations reduced energy gains by 13.3 % and 36.7 %, respectively with respect to the SW configuration .Whereas on the coldest day they reduced losses by 6 % and 8 %.

– The TW configuration had the best thermal performance for all orientations, since on the warmest day it reduced the total heat flux by up to 35.9 %.

– From the annual thermal evaluation of the TW configuration, on the warmest days the west orientation presents the highest values of temperature (32 °C – 36.5 °C) and heat flux (314.2 W/m^2 – 679.1 W/m^2) since the increase of solar radiation on this orientation coincides with the time when the outside temperature reaches the highest values.

– On the south, east and west orientations the energy gains did not exceed 1.2 kWhm^{-2} every month and reached up to 4.5 kWhm^{-2}, specifically on the south orientation in winter, due to this, the use of multiple glazings is recommended.

– The highest value of solar radiation on the north orientation is 58.8 %, 63.5 %, and 65.7 % lower than on the south, east and west, respectively; In addition, the north orientation has a limited time of exposure to direct solar radiation during the year, due to this the use of multi-glazed such as DW or TW may not be feasible on this orientation.

References

[1] Bienvenido-Huertas, D., Sánchez-García, D., Tejedor, B., & Rubio-Bellido, C. (2023). An innovative approach to assess the limitations of characterizing solar gains in buildings: A Spanish case study. Energy and Buildings, 293, 113206. https://doi.org/10.1016/j.enbuild.2023.113206

[2] Vitro arquitectónico, 2021. https://www.vitro.com

[3] Arıcı, M., Karabay, H., & Kan, M. (2015). Flow and heat transfer in double, triple and quadruple pane windows. Energy and Buildings, 86, 394–402. https://doi.org/10.1016/j.enbuild.2014.10.043

[4] González-Julián, E., Xamán, J., Moraga, N. O., Chávez, Y., Zavala-Guillén, I., & Simá, E. (2018). Annual thermal evaluation of a double pane window using glazed available in the Mexican market. Applied Thermal Engineering, 143, 100–111. https://doi.org/10.1016/j.applthermaleng.2018.07.053

[5] Heydari, A., Sadati, S. H., & Gharib, M. R. (2021). Effects of different window configurations on energy consumption in building: Optimization and economic analysis. Journal of Building Engineering, 35, 102099. https://doi.org/10.1016/j.jobe.2020.102099

[6] Yang, X., Liu, D., Yang, R., Ma, Y., Tong, X., Wu, Y., & Arıcı, M. (2023). Comprehensive performance evaluation of double-glazed windows containing hybrid nanoparticle-enhanced phase change material. Applied Thermal Engineering, 223, 119976. https://doi.org/10.1016/j.applthermaleng.2023.119976

[7] Yamaç, H. İ., & Koca, A. (2023). Investigation of water flow window with/without energy storage tank during winter season. Applied Thermal Engineering, 225, 120164. https://doi.org/10.1016/j.applthermaleng.2023.120164

[8] Huang, Y., Mankibi, M. E., & Cantin, R. (2023). Thermal performance characterization of supply-air double windows: A new guarded hot box protocol and numerical modelization. Energy and Buildings, 287, 112993. https://doi.org/10.1016/j.enbuild.2023.112993

[9] Djamel, Z., & Noureddine, Z. (2017). The Impact of Window Configuration on the Overall Building Energy Consumption under Specific Climate Conditions. Energy Procedia, 115, 162–172. https://doi.org/10.1016/j.egypro.2017.05.016

[10] Kahsay, M. T., Bitsuamlak, G., & Tariku, F. (2020). Effect of window configurations on its convective heat transfer rate. Building and Environment, 182, 107139. https://doi.org/10.1016/j.buildenv.2020.107139

[11] Kaasalainen, T., Mäkinen, A., Sandén, T., Moisio, M., & Vinha, J. (2020). Architectural window design and energy efficiency: Impacts on heating, cooling and lighting needs in Finnish climates. Journal of Building Engineering, 27, 100996. https://doi.org/10.1016/j.jobe.2019.100996

[12] Amaral, A. C. F., Rodrigues, E., Gaspar, A. R., & Gomes, Á. (2016). A thermal performance parametric study of window type, orientation, size and shadowing effect. Sustainable Cities and Society, 26, 456–465. https://doi.org/10.1016/j.scs.2016.05.014

[13] Arıcı, M., Tükel, M., Yıldız, Ç., Li, D., & Karabay, H. (2020). Is the thermal transmittance of air-filled inclined multi-glazed windows similar to that of vertical ones? Energy and Buildings, 229, 110515. https://doi.org/10.1016/j.enbuild.2020.110515

[14] Rodríguez-Ake, A., Xamán, J., Hernández-López, I., Sauceda, D., Carranza-Chávez, F. J., & Zavala-Guillén, I. (2022). Numerical study and thermal evaluation of a triple glazing window under Mexican warm climate conditions. Energy, 239, 122075. https://doi.org/10.1016/j.energy.2021.122075

[15] ASHRAE – American Society of Heating. Refrigeration and air conditioning engineers. Handbook of fundamentals; 2001. https://www.ashrae.org/technical-resources/ashrae-handbook

[16] Zhang, C., Gang, W., Wang, J., Xu, X., & Du, Q. (2019). Numerical and experimental study on the thermal performance improvement of a triple glazed window by utilizing low-grade exhaust air. Energy, 167, 1132–1143. https://doi.org/10.1016/j.energy.2018.11.076

[17] WINDOW, Lawrence Berkeley National Laboratory, 2019. https://windows.lbl.gov

[18] Xamán, J., Álvarez, G., Lira, L., & Estrada, C. (2005). Numerical study of heat transfer by laminar and turbulent natural convection in tall cavities of façade elements. Energy and Buildings, 37(7), 787–794. https://doi.org/10.1016/j.enbuild.2004.11.001